PIER C

(Received 12 March 2025, Accepted 21 April 2025, Scheduled 7 May 2025)

Design of Sparse Wideband Frequency-Invariant Beamforming Based on Hybrid Grey Wolf – l_∞-Norm Algorithm

Guihan Xie, Bin Wang*, and Kui Tao

College of Electronic Engineering & Institute for Advanced Sciences
Chongqing University of Posts and Telecommunications, Chongqing, China

ABSTRACT: A novel hybrid algorithm is proposed for frequency-invariant (FI) beam pattern synthesis of wideband nonuniformly spaced array (NUSA), which combines intelligent optimization algorithm with convex optimization algorithm. The improved grey wolf optimization (IGWO) algorithm is employed to optimize the positions of the array elements, while l_∞-norm is introduced to describe spatial response variation (SRV) for optimizing the finite impulse response (FIR) filter weights of the array. Considering multiple constraints, such as array aperture and minimum spacing between elements, an optimal trade-off among constant beamwidth, FI characteristics, and peak sidelobe level (PSL) is achieved. The effectiveness and advantages of this method are evidenced by synthesis examples of FI beam patterns for wideband NUSA in different application scenarios. These experimental results hold important theoretical significance, and provide valuable references for solving the optimization problem of wideband FI array under multiple constraints.

1. INTRODUCTION

Wideband frequency-invariant beamforming arrays have garnered significant attention due to their ability to maintain waveform integrity when receiving wideband signals. In recent years, multiple convex optimization techniques have been introduced for the synthesis of frequency-invariant (FI) beam patterns in uniform wideband arrays, such as the harmonic nesting method [1], Fourier transform method [2, 3], spatial response variation (SRV) description using the l_∞-norm [4], the alternating direction method of multipliers (ADMM) [5], and second-order cone programming (SOCP) [6]. Compared to uniform arrays, nonuniform sparse arrays (NUSAs) offer greater freedom in element positioning, avoid grating lobes, and achieve superior radiation performance [7]. Moreover, the use of fewer array elements enables smaller system size, lower manufacturing costs, and reduced power consumption. Meanwhile, NUSA is widely applicable in direction-finding [8], radar [9], and wireless communications [10, 11]. Therefore, by simultaneously optimizing the filter coefficients and the element positions in NUSA, FI beam pattern synthesis under multiple constraints can be achieved to suit a broader range of application scenarios.

Over the last several decades, a series of advanced techniques have been proposed for synthesizing wideband FI NUSA arrays, such as the earlier harmonic nesting method [12] and direct analysis method [13]; more optimization parameters of compressed sensing [14], l_1 norm method [15], and matrix beam method [16] can be considered; second-order cone programming (SOCP) [17, 18] and alternating projection approach (APA) [19] with fast convergence rate are also popular in recent years. All of these methods are designed to realize wideband FI patterns by optimizing the NUSA and element excitation weight, which are particularly effective for decreasing the number of elements and meeting FI. However, multiple constraints may need to be satisfied by optimizing either excitation weights or element positions. These constraints may include enhancing SRV characteristics, narrowing beamwidth, suppressing sidelobe levels (SLLs), defining array aperture, and ensuring sparse element placement, which are crucial considerations in array design. While this is an important issue, discussions on such NUSA cases are relatively scarce.

In this paper, we focus on synthesizing wideband NUSA with constant beamwidth, minimal sidelobes, and a main lobe FI beam pattern under a given array aperture. To achieve this, the choice of optimization method is determined by the difficulty of transforming the constrained problem into a convex problem. Researchers have developed various practical synthesis methods to address the FI beam pattern synthesis problem with constant beamwidth and sidelobe levels in convex optimization. Among them, the method proposed in [4], which uses the l_∞-norm to design uniform wideband arrays with FI pattern requirements, is characterized by low variance and good optimization performance. This method is referenced in this paper to describe SRV characteristics, and a relaxation-based optimization method is proposed to minimize sidelobe levels in wideband beam patterns.

Due to the high mathematical modeling difficulty of solving position optimization problems using convex optimization and the challenge of balancing exact and approximate solutions, it is necessary to consider alternative optimization methods. Intelligent optimization algorithms are an excellent choice due to their superior global search capabilities and ability to handle multimodal and nonlinear problems. In 2014, the Grey Wolf Op-

* Corresponding author: Bin Wang (wangbin1@cqupt.edu.cn).

timizer (GWO) algorithm was first proposed [20]. Compared to multi-objective evolutionary algorithms [21] and modified competitive swarm optimizer [22], GWO algorithm has been widely applied in a variety of optimization applications due to its simplicity, few parameters, ease of programming, and strong global search ability. In array synthesis, GWO algorithm has been applied to sparse array [23], conformal arrays [24], linear arrays [25], and rectangular array [26]. Although GWO algorithm has demonstrated good performance in practical applications, it also faces several challenges. For example, when solving nonlinear problems, the algorithm lacks population diversity and tends to get trapped in local optima. Its ability to escape local optima in later iterations is also limited. However, as addressed in [26] and [27], this issue was well solved by using Tent chaotic mapping. Therefore, this communication introduces this method and applies an improved GWO algorithm for position optimization. A collection of examples was conducted for various wideband FI patterns. These examples encompass comparisons with other methods.

In this paper, a hybrid algorithm combining IGWO with l_∞-norm is proposed for the synthesis of wirelessly bound linear arrays under multiple constraints. The method optimizes the element position and excitation amplitude, and effectively reduces the PSL of sparse array under the condition of frequency invariance. First, the hybrid approach has two parts. In the first part, GWO is improved.

1) The inherent chaotic disorder and ergodicity in the initialization process are used to improve the degree of freedom of array position.

2) Nonlinear rounding strategy is adopted to improve the algorithm by introducing the number of iterations into the convergence factor, and the convergence degree can be adjusted according to the iteration situation. This method not only improves the global search ability of the algorithm, but also avoids the possibility of falling into the local optimal.

3) In the process of location update of grey Wolf optimization algorithm, a dominant Wolf dynamic confidence strategy is proposed to improve population diversity and search efficiency by adjusting individual voice.

4) When the algorithm is stuck in convergence stagnation, the opposing learning strategy is introduced to help the algorithm jump out of the current solution and find other optimal solutions.

By improving the GWO, the efficiency and search accuracy of the GWO in the sparse array position optimization are improved. In the second part, in the case of sparse distribution based on IGWO, convex optimization algorithm based on l_∞ norm is used to solve the excitation amplitude optimization scheme under the minimum PSL target with FI characteristics, in order to increase the computational efficiency and accuracy of the problem description. Therefore, the hybrid algorithm proposed in this paper can reduce the number of array elements, while maintaining certain radiation characteristics with broadband frequency invariance, thus reducing the system cost.

The innovation of this paper lies in proposing a hybrid optimization framework that, for the first time, integrates IGWO algorithm (for global rapid search of element spacing) with convex optimization (for local precise solving of element excitation) to address the FI multi-objective optimization problem in broadband NUSA. Compared to single-strategy optimization approaches (e.g., using only intelligent algorithm or convex optimization alone), the hybrid algorithm achieves the following advantages through hierarchical decoupling of optimization variables:

1) Global-local collaborative optimization. IGWO avoids local optima in spacing optimization, while convex optimization ensures accurate excitation solutions.

2) Computational efficiency is improved. The hybrid framework reduces dimensionality and iteration counts compared to traditional intelligent algorithm full-variable optimization.

3) Broadband constraint is satisfied. Explicit constraint modeling via convex optimization ensures strict adherence to frequency-domain response requirements, circumventing the constraint relaxation issues inherent in heuristic algorithms.

The rest of this article is structured as follows. Section 2 provides a linear FIR sparse array signal model. Section 3 introduces the algorithm model of array excitation optimization. Section 4 introduces the GWO improvement strategy, the algorithm model of array position optimization, and the general flow of the hybrid algorithm. In Section 5, numerical simulation results and comparative analysis are presented to validate the proposed method. Finally, Section 6 gives the conclusion of this paper.

2. LINEAR FIR SPARSE ARRAY SIGNAL MODEL

Consider a symmetric far-field linear wideband beamformer array model placed along the X-axis, with an aperture of L_a as shown in Figure 1. The array model is divided into two categories: odd arrays, which are symmetric about the center element, and even arrays, which are symmetric about the midpoint of the two central elements. Each isotropic element is followed by a finite impulse response (FIR) filter, with the filter's tap length denoted as L, and the vector of filter coefficients is represented as:

$$\mathbf{w}_m = [w_{m,0}, w_{m,1}, \cdots, w_{m,L-1}]^T \tag{1}$$

where $w_{m,l}$ denotes the lth coefficient of the mth FIR filter, and $[\cdot]^T$ represents the transpose. For the even symmetric wideband beamformer array, the vector of weight coefficients can be rep-

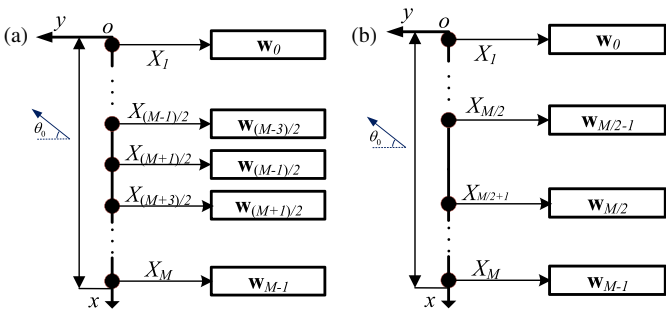

FIGURE 1. Wideband linear beamformer structure. (a) Odd array. (b) Even array.

resented as:

$$\mathbf{w} = \left[\mathbf{w}_0^T, \mathbf{w}_1^T, \cdots, \mathbf{w}_{M-1}^T\right]^T \tag{2}$$

Accordingly, the array response of the beamformer can be expressed as a function of the signal frequency f and the incident angle θ:

$$\mathbf{P}(f,\theta) = \sum_{m=1}^{M}\sum_{l=1}^{L} w_{m,l} e^{-j2\pi f(d_m \cos(\theta)/c + (l-1)/f_s)} \tag{3}$$

where d_m is the distance of the mth element relative to the reference element. Assuming that the first element is the reference, the distance of the mth element relative to the first element is $d_m = X_m - X_1$. X_m denotes the coordinate of the mth element, c the speed of sound in air, f_s the signal sampling frequency, and j the imaginary unit. Set:

$$\mathbf{g}(f,\theta) = \left[e^{-j2\pi f d_1 \cos(\theta)/c}, \cdots, e^{-j2\pi f d_M \cos(\theta)/c}\right]^T \tag{4}$$

$$\mathbf{e}(f) = \left[1, \cdots, e^{-j2\pi f(L-1)/f_s^T}\right]^T \tag{5}$$

the array steering vector can be expressed as:

$$\mathbf{s}(f,\theta) = \mathbf{g}(f,\theta) \otimes \mathbf{e}(f) \tag{6}$$

where $\otimes$ denotes the Kronecker product of the matrices. Accordingly, Equation (3) can be simplified as:

$$\mathbf{P}(f,\theta) = \mathbf{s}^T(f,\theta)\mathbf{w} \tag{7}$$

in this way, the original array response can be divided into steering vector and exciting vector, and expressed in matrix form, which can simplify the modeling of complex system and is more conducive to analysis and design.

3. EXCITATION OPTIMIZATION

The introduction of excitation optimization primarily aims to optimize the PSL of the wideband beam pattern while controlling the beamwidth and maintaining frequency invariance.

The definition of the maximum peak sidelobe level between different frequencies is as follows:

$$\mathrm{PSLL}_1 = \max\left\{\left|\frac{\mathbf{P}_{\max}(f_i,\theta_s)}{\mathbf{P}_{\max}(f_i,\theta_j)}\right|\right\} \tag{8}$$

where $i = 1, ..., I$, where I is the number of sampling points within the frequency range. $j = 1, ..., J$, where J is the number of sampling points within the passband angular range of the visible area Θ. θ_s denotes the passband angular range set within the sidelobe region.

It is well known that methods based on SRV constraints are representative approaches in the design of frequency invariance. In [4], SRV is described using the l_∞-norm, which is represented in the following form:

$$\begin{aligned}\overline{\mathrm{SRV}}_\infty &= \max_{f_i\in[f_{\min},f_{\max}],\theta_{j\in\theta^{\mathrm{FI}}}} \left|\mathbf{w}^H\mathbf{s}(f_i,\theta_j) - \mathbf{w}^H\mathbf{s}(f_r,\theta_j)\right| \\ &= ||\mathbf{d}(\mathbf{w})||_\infty^{\theta^{\mathrm{FI}}}\end{aligned} \tag{9}$$

where $\|\cdot\|_\infty$ denotes the l_∞ norm, and θ_{FI} represents the angular range in which the FI characteristics are expected to be maintained. Generally, after maintaining FI characteristics within θ_{FI}, the actual first null point of the main beam will still deepen and widen outward. Therefore, the actual main beam range obtained is typically larger by about 2° to 3°. Furthermore, to synthesize the FI beam pattern, $\overline{\mathrm{SRV}}_\infty$ must be sufficiently small to limit the expected fluctuations of the array's spatial response in the desired frequency band. Besides, to avoid trivial solutions, a response constraint condition is introduced for the desired direction θ_0. The final relaxed constraint representation of the wideband beam pattern in the spatial domain is expressed as:

$$\begin{aligned}&\min\ \mathrm{PSLL}_1 \\ &s.t. \quad \left|\mathbf{s}^T(f,\theta_0)\mathbf{w}^H\right| = 1 \\ &\quad\ ||\mathbf{d}(\mathbf{w})||_\infty^{\theta_{\mathrm{FI}}} \le \varepsilon\end{aligned} \tag{10}$$

At present, there are many mature solvers for solving convex optimization problems. In this paper, CVX toolbox of Matlab [30] is selected to solve Equation (10).

4. POSITION OPTIMIZATION

In this section, the optimization objective is considered based solely on the positions of the array elements. Accordingly, the signal optimization model can be simplified as:

$$\hat{\mathbf{P}}(f,\theta) = \mathbf{g}^T(f,\theta)\mathbf{w} \tag{11}$$

To reduce the PSL within the passband, the PSL at both the minimum and maximum frequencies needs to be used as factors in the fitness function. The fitness function of the IGWO is as follows:

$$\mathrm{PSLL}_2 = \max\left\{\left|\frac{\hat{\mathbf{P}}_{\max}(f_1,\theta_s)}{\hat{\mathbf{P}}_{\max}(f_1,\theta_k)}\right|, \left|\frac{\hat{\mathbf{P}}_{\max}(f_P,\theta_s)}{\hat{\mathbf{P}}_{\max}(f_P,\theta_k)}\right|\right\} \tag{12}$$

Under multiple constraint conditions such as array aperture, number of elements, and the minimum spacing between elements, the expression for the multi-constraint conditions of sparse linear array is as follows:

$$\begin{aligned}&\min\ \mathrm{PSLL}_2 \\ &s.t. \quad |X_m - X_{m-1}| \ge d_{\min} \\ &\quad\ X_1 = 0, X_M = L_a \\ &\quad\ L_a = \tfrac{\lambda_U}{2}\left\lceil M \times (\eta_L + 1) - 1\right\rceil\end{aligned} \tag{13}$$

where $d_{\min}$ represents the minimum element spacing constraint, set to half of the wavelength at the maximum frequency ($d_{\min} = \lambda_U/2$). The search range for X_m is [0, L_a]. X_m can be expressed as $X_m = \sum_{i=1}^{m} x_i + (m-1)d_{\min}$. x_m denotes the distance between elements after removing $d_{\min}$, with a value range of $[0, L_a - (M-1)d_{\min}]$. The schematic diagram of the element distribution of the array is shown in Figure 2.

In Equation (13), given a fixed number of elements, the size of the array aperture is initialized using a half-wavelength uniform array, where the half-wavelength is selected as the wave-

TABLE 1. IGWO optimization of 10 array elements with different η_L.

η_L	PSL with f_L	PSL with f_U	FNBW with f_L	FNBW with f_U	Number of convergence iterations	Convergence time (s)
0.1	−16.2509 dB	−16.2527 dB	36.00°	11.00°	21	12.90
0.2	−18.2657 dB	−18.2142 dB	33.00°	11.00°	32	19.47
0.3	−17.6027 dB	−16.2283 dB	30.00°	10.00°	38	19.35
0.4	−15.7191 dB	−15.7236 dB	27.00°	9.00°	33	18.85

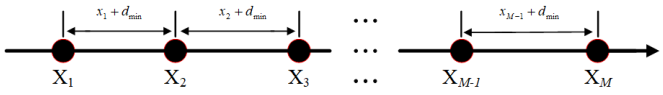

FIGURE 2. Broadband line bursts distribution diagram.

length at the maximum frequency. The array conversion coefficient (ACC) η_L is then determined, which takes on non-negative values, where $\lceil\cdot\rceil$ denotes the ceiling function. Since the excitation of the array requires a specified number of elements, the desired number of elements can be freely adjusted under the fixed array aperture using ACC.

4.1. Determination of the Fitness Function for the IGWO Algorithm

In GWO algorithm, the optimization results correspond to four types of individuals: the historical optimal solution is defined as α, the second-best solution as β, the third-best solution as δ, and the candidate solution as ω. Assuming that the gray wolf population is denoted as M_p, each population consists of M gray wolves. The position of the mth gray wolf in the solution space can be represented as $x_m = \left(x_{m,1}, x_{m,2}, \cdots, x_{m,M_p}\right)$. The fitness function can be represented as:

$$\text{Fit} = \begin{bmatrix} \text{PSLL}_2\left([x_{1,1}\ x_{2,1}\ \cdots\ \cdots\ x_{M,1}]\right) \\ \text{PSLL}_2\left([x_{1,2}\ x_{2,2}\ \cdots\ \cdots\ x_{M,2}]\right) \\ \vdots\quad \vdots\quad \vdots\quad \vdots\quad \vdots \\ \text{PSLL}_2\left([x_{1,M_p}\ x_{2,M_p}\ \cdots\ \cdots\ x_{M,M_p}]\right) \end{bmatrix} \tag{14}$$

The gray wolves are classified based on the magnitude of the fitness values, sequentially selecting the leaders $(X_\alpha, X_\beta, X_\delta)$ for the subsequent hunting process.

4.2. Population Initialization Based on Tent Chaotic Mapping

To address the issue of uneven initialization distribution, a Tent chaotic mapping with highly random characteristics is used to generate an initial population with a wide distribution [26, 27], which improves the original GWO to IGWO.

First, a random control variable is added during its use:

$$Z_{i+1} = \begin{cases} 2Z_i + \text{rand}(0,1)/M_p t_{\max}, & 0 \le Z \le 1/2 \\ 2(1-Z_i) + \text{rand}(0,1)/M_p t_{\max}, & 1/2 \le Z \le 1 \end{cases} \tag{15}$$

where $t_{\max}$ is the maximum number of iterations. Next, perform a Bernoulli transformation on Equation (15):

$$Z_{i+1} = (2Z_i)\text{mod}1 + \text{rand}(0,1)/M_p t_{\max} \tag{16}$$

where mod denotes the modulus operation. Since the search scale of the algorithm varies with different problems, it is essential to provide chaotic sequences with enhanced diversity and problem-specific characteristics.

After generating the chaotic variable Z_{i+1} from Equation (16), it will be introduced into the optimization model to generate the initial population:

$$x^0 = l_b + (U_b - l_b) \cdot Z_{i+1} \tag{17}$$

l_b and U_b represent the minimum and maximum values of the position variable x.

4.3. Position Update Method

In IGWO, gray wolves of ω adjust their position to gradually approach the prey of each generation. Before this, A and C are introduced to simulate the behavior of wolves gradually surrounding their prey, expressed as:

$$A = 2a \cdot \text{rand}(0,1) - a \tag{18}$$

$$C = 2 \cdot \text{rand}(0,1) \tag{19}$$

where $\text{rand}(0,1)$ is a random number in the range of [0, 1), and a is the convergence factor, which is given by:

$$a = 2 \times \left[1 - \left(\frac{1}{\text{e}^{(t/t_{\max})^3}} - 1\right) \cdot \frac{\text{e}}{1-\text{e}}\right] \tag{20}$$

Such parameter settings can dynamically change according to the early, middle, and late stages of the algorithm, which is beneficial for global search and also alleviates the possibility of getting trapped in a local optimum.

The distance and updated position between the leadership wolves and other gray wolves are as follows:

$$D = |C \cdot X_p(t) - X(t)| \tag{21}$$

$$X(t+1) = X_p(t) - A \cdot D \tag{22}$$

By introducing the positions of X_α, X_β, and X_δ, the position evaluation of the current iteration number can be obtained as X_1, X_2, X_3, respectively. Leadership abilities of gray wolves at different orders in the gray wolf population are different, which depends on the variation of fitness function values from

different iterations.

$$\begin{cases} \eta_1 = \eta_{\max} - (t/t_{\max}) \cdot [(\eta_{\max} - \eta_{\min})/2] \\ \eta_2 = (\eta_{\max} + \eta_{\min})/2 \\ \eta_3 = \eta_{\min} + (t/t_{\max}) \cdot [(\eta_{\max} - \eta_{\min})/2] \\ X(t+1) = X_1(t) \cdot \eta_1 + X_2(t) \cdot \eta_2 + X_3(t) \cdot \eta_3 \end{cases} \tag{23}$$

where η_1, η_2, and η_3 are the weight values of α, β, and δ wolves. $\eta_{\max}$ and $\eta_{\min}$ are the maximum and minimum weights, respectively, taken as 4/9 and 2/9.

When the algorithm falls into convergence stagnation, some gray wolves with lower fitness function values are mutated according to their fitness function values, and the mutation rule introduces an oppositional learning strategy to increase the diversity of the gray wolf population and improve the iteration efficiency [28]. The mathematical expression for the adversarial learning strategy in [29] is as follows:

$$\hat{X}(t) = l + U - \text{rand}(0,1) \cdot X(t) \tag{24}$$

where U and l are the upper and lower boundaries of $X(t)$.

5. ANALYSIS OF SIMULATION RESULTS

In this section, in order to avoid temporal and spatial aliasing, we keep the minimum spacing between array elements as $0.5\lambda_U$, $f_s = 2f_U$. In addition, in IGWO algorithm, we set the maximum number of iterations $t_{\max} = 100$ and population size of gray wolves $M_p = 200$. The number of sampling points are set to $J = 181$, and $I = 16$, respectively. Since the arrays optimized in this paper are all symmetric arrays, half of the arrays can be optimized directly, and the rest is obtained by pairwise display. The distance between the two array elements at the center of the symmetric even array is set to $0.5\lambda_U$.

In different experiments, only the number of array elements M and η_L are changed. Each simulation example is run on an AMD Ryzen 7 5700G with Radeon Graphics 3.80 GHz computer.

In order to evaluate the obtained FI properties, a parameter defined in [3] is introduced. This parameter is called frequency variation factor (FVF) and is given by:

$$\sigma = \sqrt{\frac{1}{PK} \sum_{p=0}^{P-1} \sum_{k=0}^{K-1} \left\{ 20 \log \left| \mathbf{P}(f_p, \theta_k^{\text{FI}}) \right| - \mu(\theta_k^{\text{FI}}) \right\}^2} \tag{25}$$

$$\mu(\theta_k^{\text{FI}}) = \frac{1}{P} \sum_{p=0}^{P-1} 20 \log \left| P(f_p, \theta_k^{\text{FI}}) \right| \tag{26}$$

where $p = 0, ..., P-1$, P is the number of sampling points of the frequency range, and $k = 0, ..., K-1$, K is the number of sampling points of θ.

5.1. Wideband Nonuniform Array Synthesis with Constant Sidelobe Level Based on IGWO

The first example has the same parameter settings as [19] for ease of comparison with it. Array position optimization will be performed for a linear array with 10 isotropic array elements.

Algorithm 1 The main steps of the hybrid algorithm for NUSA wideband FI beampattern synthesis (Continue)

1: Define the population size of the grey wolf M_p, the largest number of iteration $t_{\max}$, the number of grey wolf individuals M, the minimum spacing $d_{\min}$, the array transform factor η_L, high and low bounds U_b, l_b of grey wolf individuals;

2: Initialize the population: initial populations are generated using the tent chaos mapping by equation (15), (16) and (17); Calculation of the fitness function value Fit for the individuals in the population;

3: **while** $t \le t_{\max}$ **do**

4: get α, β and δ positions X_α, X_β and X_δ;

5: **for** $i = 1 : N_P$ **do**

6: Update A, C, a by equation (18), (19) and (19);

7: Update grey wolf positions by equation (21),(22) and (23);

8: **end for**

9: Calculation of fitness function values of the new generation of grey wolf populations, the newly obtained individuals are compared with the previous ones and the better results are retained. Get α, β and δ positions X_α, X_β and X_δ

10: Check if it is falling into convergence stagnation, and if so, update the grey wolf position by equation (24);

11: Calculation of fitness function values for the new generation of grey wolf populations;

12: The newly obtained individuals are compared with the previous ones and the better results are retained;

13: $t = t + 1$;

14: **end while**

15: Output the optimal array position distribution solution;

16: The excitation of the array is optimized according to equation (10);

17: Output the optimal array excitation distribution solution.

Set $\eta_L = 0.1$, according to Equation (16). $L_a = 5\lambda_U$ can be calculated. It is expected to achieve a constant sidelobe level in $\Omega \in [0.4, 1.2]$ GHz, and the beam center is set to $\theta_0 = 0°$.

According to the set array position requirements as well as the population size and the number of iterations according to the Figure 3(a), it is known that the IGWO algorithm can achieve stable optimization results after 21 iterations. As shown in Figure 4, the position of the array elements is optimized under the requirements of array aperture and minimum spacing, and the spacing of the array elements is gradually increased from the center to the sides.

By IGWO, the optimization of the array element position has a faster convergence speed, but since the array aperture is set smaller here, the space available for optimization is also smaller. Therefore, the optimization of the sidelobe level is not obvious by directly using the IGWO method. Changing the ACC to 0.2, as shown in Figure 3(b), the optimization of

TABLE 2. Optimization results of IGWO algorithm based on different wavelength reference.

Wavelength reference	PSL with f_L (dB)	PSL with f_U (dB)	FNBW with f_L	FNBW with f_U	Gain with f_L (dBi)	Gain with f_U (dBi)
f_L	-13.33	-4.27	11.00°	4.00°	13.22	12.94
$(f_L + f_U)/2$	-12.93	-13.06	20.00°	7.00°	10.68	14.92
f_U	-16.25	-16.25	36.00°	11.00°	8.80	13.36

TABLE 3. Optimization results of hybrid algorithm based on different wavelength reference.

Wavelength reference	PSL with f_L (dB)	PSL with f_U (dB)	FNBW	Gain with f_L (dBi)	Gain with f_U (dBi)	FVF (dB)
f_L	-5.88	-5.86	22.00°	8.24	8.35	0.5341
$(f_L + f_U)/2$	-8.87	-8.87	18.00°	9.91	9.87	0.5204
f_U	-18.51	-18.53	18.00°	11.44	11.2	0.2387

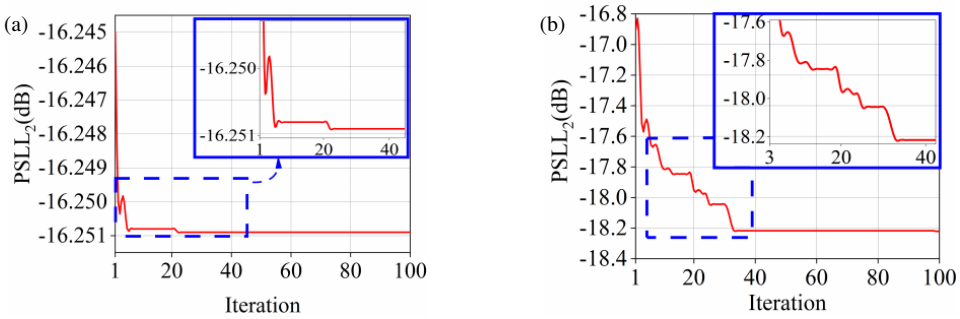

FIGURE 3. 10 array element IGWO iteration cases. (a) $\eta_L = 0.1$. (b) $\eta_L = 0.2$.

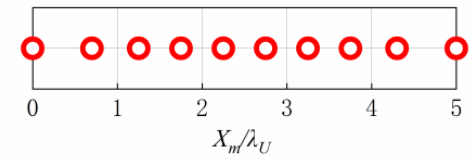

FIGURE 4. 10-array element NUSA layout (λ_U is the wavelength at f_U).

constant sidelobe level is achieved in 31 iterations. It can be seen that there are waveform ups and downs during the IGWO optimization process, demonstrating the optimization back and forth between the minimum frequency point and maximum frequency point. As shown in Figure 3(b) and Table 1, the optimization of PSL by IGWO is better in the case of 10 array elements with ACC $= 0.2$, which can be chosen independently according to the requirements of aperture efficiency and optimization time. The case of ACC $= 0.1$ with the least optimization time will be chosen later for the consideration of optimization rate.

The optimized directional pattern results are shown in Figures 5(a) and (b). With f_L and f_U, the difference of first null beamwidth (FNBW) is large, but PSL variation (ΔPSL) is small, which basically realizes the optimization of constant sidelobe level.

The wavelength reference in the aforementioned experiments was selected based on the maximum frequency, as higher-frequency signals with shorter wavelengths are more susceptible to grating lobe formation. Consequently, adopting the highest-frequency wavelength (λ_U) as the reference enables more effective PSL suppression across the entire frequency band. For comparative analysis, we present experimental results using both the minimum-frequency wavelength (λ_L) and center-frequency wavelength (λ_0) as alternative references, thereby providing justification for selecting λ_U as the optimal reference. This is consistent with the setting of most references.

As shown in Figure 6 and Table 2, these are the pattern results obtained by the IGWO algorithm under different wavelength references. It can be observed that selecting λ_U as the wavelength reference yields better PSL performance. However, this comes at the expense of increased FNBW and reduced gain. Nevertheless, the improved PSL performance proves more advantageous for subsequent convex optimization processes.

As detailed in Table 3, the results demonstrate that selecting λ_U as the wavelength reference achieves optimal performance in terms of PSL, gain, and **FVF**. This superiority stems from the minimal ΔPSL obtained through IGWO optimization, which effectively maintains pattern consistency.

In contrast, when using λ_L as the reference, the significant grating lobe effect at high frequencies (with ΔPSL reaching 9.05 dB) leads to substantially degraded performance. Even after implementing excitation optimization and broadening the FNBW to 22°, both PSL and FVF fail to reach satisfactory levels.

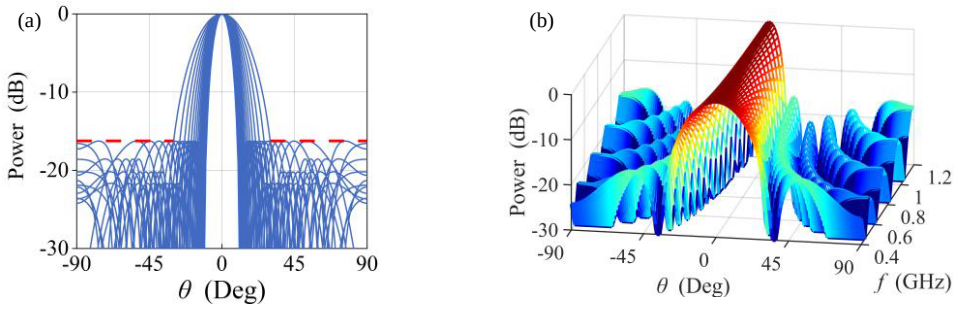

FIGURE 5. 10-element wideband uniform SLL pattern based on IGWO algorithm. (a) IGWO joint spatial frequency distribution and (b) IGWO orientation map at discrete frequencies.

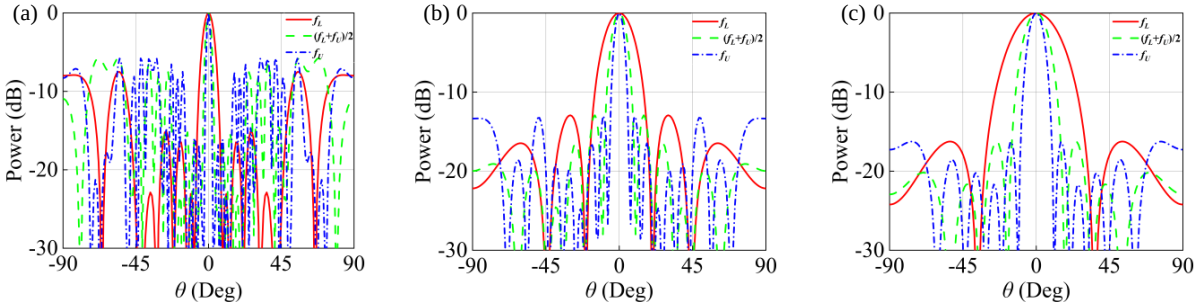

FIGURE 6. The uniform SLL pattern obtained by IGWO algorithm with the wavelength reference (a) λ_L; (b) λ_0; (c) λ_U.

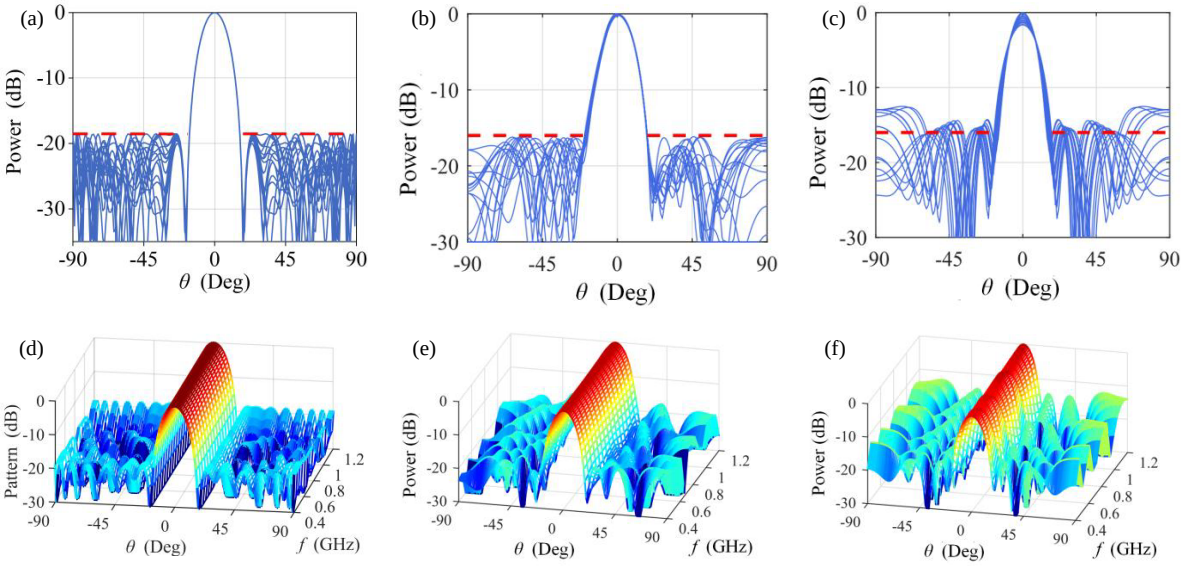

FIGURE 7. Uniform SLL wideband FI beam pattern based on (a) and (d) the proposed hybrid algorithm; (b) and (e) generalized APA [19]; (c) and (f) ATD [7].

5.2. Focused FI Beam Pattern with Constant Beamwidth Based on Hybrid Algorithm

This example will use convex optimization for the array element excitation in the case of the array position optimized in experiment 1. The relevant parameters are also set the same as in [19]. The expectation of maintaining the FI characteristics is set within $\Omega \in [0.4, 1.2]$ GHz; the reference frequency $f_r = (f_L + f_U)/2$; and the beam center is set to $\theta_0 = 0°$. The upper bound of the l_∞-SRV constraints is defined as $\varepsilon = 5 \times 10^{-3}$. The constraint region will be set to $[-14°, 14°]$ with the sidelobe region as $[-90°, -14°] \cup [14°, 90°]$.

Figures 7(a) and (d) show the pattern obtained by the hybrid algorithm. By optimizing the excitation of array elements through the l_∞ convex optimization algorithm, FI characteristics can be effectively achieved. The width of the main beam in the passband is constant at 18°, and the value of the FVF is 0.2387 dB. While favorable FI characteristics are achieved, good PSL suppression can also be obtained. The PSL with f_L

TABLE 4. Comparison of focused FI beam optimization results based on different algorithms.

Synthesis Method	PSL (dB)	FNBW	FVF (dB)	Convergence number
Hybrid Algorithm	-18.51	18.00°	0.24	21
Convex optimization	-18.38	18.00°	0.28	-
Generalized APA [19]	-16.07	18.00°	0.28	48
ATD [7]	-12.52	18.00°	1.01	-
SSA [27]	-16.94	18.00°	0.32	13
GA [31]	-16.35	18.00°	0.23	96

is -18.51 dB, and the PSL with f_U is -18.53 dB, which is also a very small difference.

As shown in Figure 7 and Table 4, the beam shape synthesized by the hybrid optimization algorithm is more regular than the generalized APA proposed in [1] and the asymptotic theory-based design (ATD) method proposed in [7]. Under the same main flap beamwidth, the FVF performance is reduced by 0.04 dB and the PSL reduced by 2.44 dB compared with the generalized APA; the FVF performance is reduced by 0.77 dB and the PSL reduced by 5.99 dB compared with the ATD method. The proposed hybrid algorithm will obtain more effective PSL suppression and better FI characteristics, which is a better optimization effect.

As indicated in Table 4, the comparison of focused FI beam optimization results based on different algorithms is presented. Specifically, only the convex optimization algorithm was applied to optimize the excitations of a uniform array (11 elements) within the same aperture. When FNBW of 18° is maintained, the PSL within the passband reaches -18.38 dB, with FVF of 0.28 dB. This demonstrates that the introduction of the IGWO algorithm reduces the number of array elements without degrading the PSL and FI performance. Furthermore, the IGWO-driven suppression of PSL variations across the operating bandwidth enhances both PSL suppression capability and FI stability, thereby synergistically improving the overall system performance. The performance gap becomes more pronounced as the number of array elements increases.

Replacing IGWO in the hybrid algorithm with SSA [27] and GA [31], respectively, resulted in inferior PSL optimization outcomes compared to IGWO, confirming IGWO's superior sidelobe suppression capability. Notably, the FVF only slightly deteriorated by 0.01 dB. In addition, the optimization efficiency through IGWO is also relatively high, with fast convergence, where the convergence number is 21. The specific optimization time is as follows: By the hybrid algorithm, the array positions of the optimization time is 12.90 s; the excitation optimization time is 66.26 s; and the total optimization time is 79.16 s.

The hybrid algorithm effectively combines IGWO's global search capability and convex optimization's local precision, thereby achieving superior overall performance and stronger synergistic collaborative capabilities.

Figure 8(a) shows the FIR filter coefficients by the hybrid algorithm and (b) shows the FIR filter coefficients by the generalized APA. In addition, (c) and (d) show the distribution of array excitation with frequency change, defined by $W(f,m) = \sum_{l=0}^{L-1} w_{m,l} e^{-j2\pi f l \Delta t}$. The excitation weights obtained by the hybrid algorithm have significant weight ups and downs at the higher orders of the filter. It implies that the higher orders of the filter are effectively utilized, which may explain better optimization results as well as longer optimization time.

Due to the inherent uncertainty of intelligent optimization algorithms, variability in the results may occur. Figure 9 illustrates the uncertainty analysis of 100 independent experimental results using the Bootstrap Monte Carlo method. As shown in Figure 9(a), the probability density peak of PSL is 27.90, corresponding to -18.50 dB, with a 97.5% confidence interval of $[-18.53, -18.47]$ dB. In Figure 9(b), the probability density peak of FVF is 73.02, corresponding to 0.27 dB, and the 97.5% confidence interval is [0.26, 0.28] dB. Both the PSL and FVF peaks align closely with the original mean values, demonstrating the reliability of the model. Furthermore, the narrow confidence intervals for both metrics validate the effectiveness and stability of the proposed methodology.

5.3. FI Angle Setting of Wideband NUSA Array Based on Hybrid Algorithm

In this section, we investigate the effect of different beam pointing directions on the performance of the proposed method. For comparison with [4], consider a nonuniform linear array with 30 array elements. Each array element is connected to a 32 order FIR filter. The FI characteristics are expected to be maintained within $\Omega \in [0.2, 0.5]$ GHz, with the reference frequency $f_r = (f_L + f_U)/2$, and the beam center is set to $\theta = -30^\circ$. The upper bound of the l_∞-SRV constraints is defined to be $\varepsilon = 10^{-3}$. The constraint region is set to $[-48^\circ, -12^\circ]$, and the sidelobe region is $[-90^\circ, -48^\circ] \cup [-12^\circ, 90^\circ]$. Here, redefine $\mathbf{g}(f,\theta)$ as $\hat{\mathbf{g}}(f,\theta)$:

$$\hat{\mathbf{g}}(f,\theta) = \left[e^{-j2\pi f d_1(\sin(\theta)-\sin(\theta_0))/c}, \cdots, e^{-j2\pi f d_{M-1}(\sin(\theta)-\sin(\theta_0))/c}\right]^T \tag{27}$$

$$\hat{\mathbf{s}}(f,\theta) = \hat{\mathbf{g}}(f,\theta) \otimes \mathbf{e}(f) \tag{28}$$

$$\tilde{\mathbf{P}}(f,\theta) = \hat{\mathbf{s}}^T(f,\theta)\mathbf{w} \tag{29}$$

In order to verify the FI performance of the beam direction map, the frequency variation error (FVE) defined in [4]

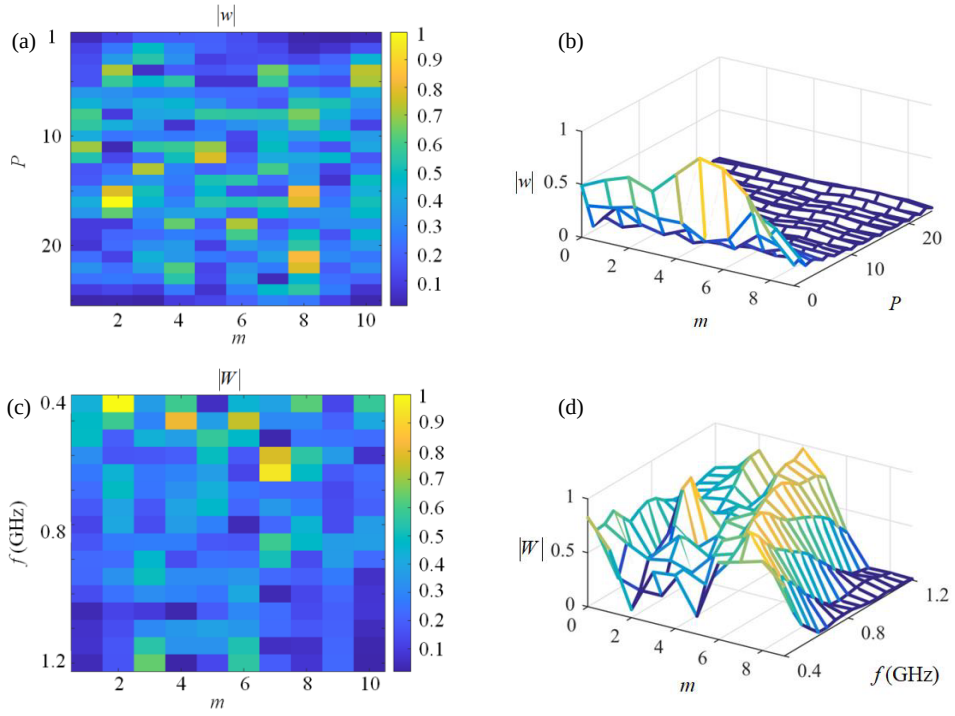

FIGURE 8. Normalized amplitudes of (a) FIR filter coefficients by the hybrid algorithm; (b) FIR filter coefficients by the generalized APA algorithm; (c) excitation weights by the hybrid algorithm; (d) excitation weights by the generalized APA algorithm.

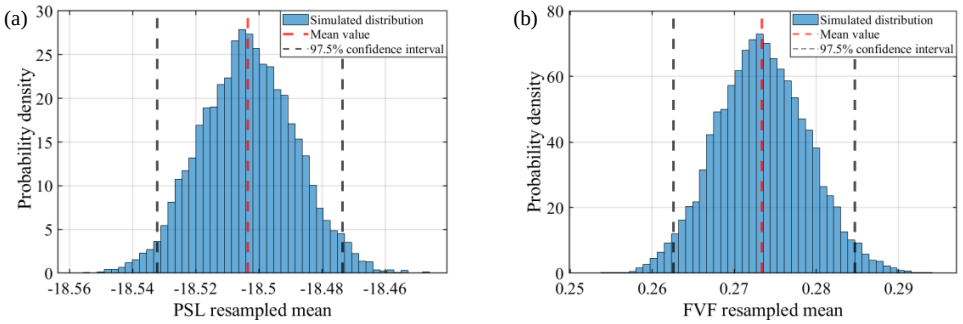

FIGURE 9. Uncertainty analysis of (a) PSL, (b) FVF based on Monte Carlo.

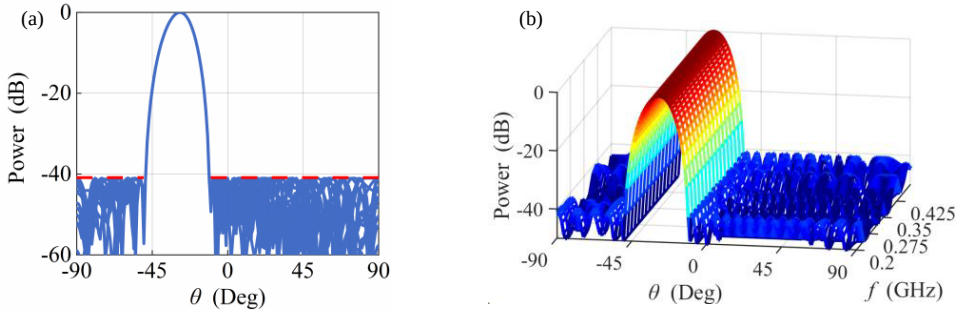

FIGURE 10. Synthesized patterns under different SRV angle setting constraints. (a) Pattern at discrete frequencies of 30 array elements. (b) 3D beam pattern for $\theta^{\mathrm{FI}} = [-50^\circ, -10^\circ]$.

is quoted as $\mu = \max_{p,k} \mu_{pk}$, where

$$\tilde{\mathbf{P}}^{\mathrm{FI}} = \left[\tilde{\mathbf{P}}_{ij}^{\mathrm{FI}}\right] = 20\log \frac{\left|\tilde{\mathbf{P}}\left(f_i, \theta_j^{\mathrm{FI}}\right)\right|}{\max\left|\tilde{\mathbf{P}}\left(f_i, \theta_j^{\mathrm{FI}}\right)\right|} \in R^{I\times J} \quad (30)$$

$$\mu_{pk} = \left\|\hat{P}_p^{\mathrm{FI}} - \hat{P}_k^{\mathrm{FI}}\right\|_2 \quad (31)$$

As shown in Table 5 and Figure 10, the main beam range is $[-50^\circ, -10^\circ]$; the PSL is -40.86 dB; the FEV is 0.45 dB;

TABLE 5. Comparison of uniform array and NUSA.

Synthesis Method	PSL (dB)	Finally Reached FNBW	FVF (dB)	FVE (dB)
NUSA Hybrid Algorithm	-40.86	$[-50.0°, -10°]$	0.24	0.45
Uniform Array l_∞-Norm Method [4]	-30.01	$[-43.0°, -17.5°]$	-	0.64

and the FVF is 0.24 dB. Compared with uniform array, the PSL is reduced by 10.85 dB and the FVE reduced by 0.19 dB. The optimization time for IGWO algorithm is 28.19 s, and the optimization time of the convex optimization algorithm is 388.13 s, which is a total of 416.32 s. In practice, this experiment employs the same angular constraint settings as [4]. However, while [4] focuses on beamwidth minimization, the proposed hybrid algorithm achieves an extended FNBW of 14.2° compared to [4], yet delivers enhanced FI stability and superior PSL suppression. This further indicates that nonuniform arrays, compared to uniform arrays, trade a controlled beamwidth expansion for significantly improved FI and PSL performance, providing a viable design strategy for scenarios requiring strict sidelobe control and frequency invariance across wide bandwidths.

6. CONCLUSION

In this paper, a hybrid algorithm is proposed for generating a wideband nonuniform FI beam pattern with restraining sidelobe level and precise main beam range control under multiple constraints. The intelligent optimization algorithm and convex optimization algorithm are efficiently fused, while taking advantage of the fast convergence of the optimal array position of the IGWO algorithm and the high efficiency of the l_∞ description of the SRV performance. The method achieves an ideal balance among beamwidth, FI characteristics, and PSL. Numerical results validate the performance of the algorithm. It is noteworthy that the proposed hybrid algorithm does not factor in the physical effects of the array, such as non-isotropic and mutual coupling effects. This may result in performance degradation under these factors. In addition, more array types and larger-scale arrays will be considered for beam formation. Meanwhile, the method can be used for the optimization of multiple-objective array antennas and multifunctional array synthesis studies. Prospective future tasks could be dedicated to address these issues.

ACKNOWLEDGEMENT

This work was supported in part by the National Natural Science Foundation of China under Grant 61601074 and in part by the Chongqing Technology Innovation and Application Development Project under Grant cstc2019jscx-msxmX0049.

REFERENCES

[1] Fang, E., C. Gui, D. Yang, and Z. Zhu, "Frequency invariant beamforming for a small-sized bi-cone acoustic vector-sensor array," *Sensors*, Vol. 20, No. 3, 661, 2020.

[2] Liu, W. and S. Weiss, "Design of frequency invariant beamformers for broadband arrays," *IEEE Transactions on Signal Processing*, Vol. 56, No. 2, 855–860, Feb. 2008.

[3] Liu, Y., L. Chen, C. Zhu, Y.-L. Ban, and Y. J. Guo, "Efficient and accurate frequency-invariant beam pattern synthesis utilizing iterative spatiotemporal fourier transform," *IEEE Transactions on Antennas and Propagation*, Vol. 68, No. 8, 6069–6079, 2020.

[4] Teng, Z., L. Gao, L. Gan, H. Liao, K. Du, and H. Jiang, "Accurate spatial-frequency response controllable frequency invariant beampattern synthesis with minimum beamwidth," *IEEE Transactions on Antennas and Propagation*, Vol. 71, No. 7, 6266–6271, 2023.

[5] Wang, W., S. Yan, and L. Mao, "Time-domain frequency-invariant beampattern synthesis via alternating direction method of multipliers," *The Journal of the Acoustical Society of America*, Vol. 147, No. 5, 3372–3375, May 2020.

[6] Yan, S., "Optimal design of FIR beamformer with frequency invariant patterns," *Applied Acoustics*, Vol. 67, No. 6, 511–528, 2006.

[7] Doles, J. H. and F. D. Benedict, "Broad-band array design using the asymptotic theory of unequally spaced arrays," *IEEE Transactions on Antennas and Propagation*, Vol. 36, No. 1, 27–33, 1988.

[8] Haupt, R. L., "Optimized element spacing for low sidelobe concentric ring arrays," *IEEE Transactions on Antennas and Propagation*, Vol. 56, No. 1, 266–268, 2008.

[9] Di Serio, A., P. Hügler, F. Roos, and C. Waldschmidt, "2-D MIMO radar: A method for array performance assessment and design of a planar antenna array," *IEEE Transactions on Antennas and Propagation*, Vol. 68, No. 6, 4604–4616, 2020.

[10] Noh, S., H. Yu, and Y. Sung, "Training signal design for sparse channel estimation in intelligent reflecting surface-assisted millimeter-wave communication," *IEEE Transactions on Wireless Communications*, Vol. 21, No. 4, 2399–2413, 2022.

[11] Gutiérrez, A. R., A. Reyna, L. I. Balderas, M. A. Panduro, and A. L. Méndez, "Nonuniform antenna array with nonsymmetric feeding network for 5G applications," *IEEE Antennas and Wireless Propagation Letters*, Vol. 21, No. 2, 346–350, 2022.

[12] Chou, T., "Frequency-independent beamformer with low response error," in *1995 International Conference on Acoustics, Speech, and Signal Processing*, Vol. 5, 2995–2998, Detroit, MI, USA, May 1995.

[13] Ward, D. B., R. A. Kennedy, and R. C. Williamson, "Design of frequency-invariant broadband far-field sensor arrays," in *Proceedings of IEEE Antennas and Propagation Society International Symposium and URSI National Radio Science Meeting*, Vol. 2, 1274–1277, Seattle, WA, USA, Jun. 1994.

[14] Hawes, M. B. and W. Liu, "Sparse array design for wideband beamforming with reduced complexity in tapped delay-lines," *IEEE/ACM Transactions on Audio, Speech, and Language Processing*, Vol. 22, No. 8, 1236–1247, 2014.

[15] Gong, Y., S. Xiao, and B. Wang, "Synthesis of nonuniformly spaced arrays with frequency-invariant shaped patterns by se-

quential convex optimization," *IEEE Antennas and Wireless Propagation Letters*, Vol. 19, No. 7, 1093–1097, 2020.

[16] Liu, Y., L. Zhang, C. Zhu, and Q. H. Liu, "Synthesis of nonuniformly spaced linear arrays with frequency-invariant patterns by the generalized matrix pencil methods," *IEEE Transactions on Antennas and Propagation*, Vol. 63, No. 4, 1614–1625, 2015.

[17] Liu, Y., L. Zhang, L. Ye, Z. Nie, and Q. H. Liu, "Synthesis of sparse arrays with frequency-invariant-focused beam patterns under accurate sidelobe control by iterative second-order cone programming," *IEEE Transactions on Antennas and Propagation*, Vol. 63, No. 12, 5826–5832, 2015.

[18] Liu, Y., J. Cheng, K. D. Xu, S. Yang, Q. H. Liu, and Y. J. Guo, "Reducing the number of elements in the synthesis of a broadband linear array with multiple simultaneous frequency-invariant beam patterns," *IEEE Transactions on Antennas and Propagation*, Vol. 66, No. 11, 5838–5848, 2018.

[19] Chen, L., Y. Liu, S. Yang, J. Hu, and Y. J. Guo, "Synthesis of wideband frequency-invariant beam patterns for nonuniformly spaced arrays by generalized alternating projection approach," *IEEE Transactions on Antennas and Propagation*, Vol. 71, No. 1, 1099–1104, 2023.

[20] Mirjalili, S., S. M. Mirjalili, and A. Lewis, "Grey wolf optimizer," *Advances in Engineering Software*, Vol. 69, 46–61, 2014.

[21] Gao, X., F. He, S. Zhang, J. Luo, and B. Fan, "A fast non-dominated sorting-based MOEA with convergence and diversity adjusted adaptively," *The Journal of Supercomputing*, Vol. 80, No. 2, 1426–1463, 2024.

[22] Gao, X., F. He, F. Wang, and X. Wang, "A modified competitive swarm optimizer guided by space sampling for large-scale multi-objective optimization," *Swarm and Evolutionary Computation*, Vol. 86, 101499, 2024.

[23] Li, X. and Y.-X. Guo, "The grey wolf optimizer for antenna optimization designs: Continuous, binary, single-objective, and multiobjective implementations," *IEEE Antennas and Propagation Magazine*, Vol. 64, No. 6, 29–40, 2022.

[24] Lv, M., J. Zhao, and J. Xu, "Pattern synthesis for sparse conformal arrays using improved grey wolf optimizer," in *2021 International Conference on Microwave and Millimeter Wave Technology (ICMMT)*, 1–3, Nanjing, China, May 2021.

[25] Li, X. and K. M. Luk, "The grey wolf optimizer and its applications in electromagnetics," *IEEE Transactions on Antennas and Propagation*, Vol. 68, No. 3, 2186–2197, 2020.

[26] Tao, K., B. Wang, X. Tian, Q. Tang, and G. Xie, "Synthesis of sparse rectangular planar arrays with weight function and improved grey wolf optimization algorithm," *IET Microwaves, Antennas & Propagation*, Vol. 18, No. 10, 748–762, 2024.

[27] Tian, X., B. Wang, K. Tao, and K. Li, "An improved synthesis of sparse planar arrays using density-weighted method and chaos sparrow search algorithm," *IEEE Transactions on Antennas and Propagation*, Vol. 71, No. 5, 4339–4349, 2023.

[28] Tizhoosh, H. R., "Opposition-based learning: A new scheme for machine intelligence," in *International Conference on Computational Intelligence for Modelling, Control and Automation and International Conference on Intelligent Agents, Web Technologies and Internet Commerce (CIMCA-IAWTIC'06)*, Vol. 1, 695–701, Vienna, Austria, Nov. 2005.

[29] Long, W., J. Jiao, X. Liang, S. Cai, and M. Xu, "A random opposition-based learning grey wolf optimizer," *IEEE Access*, Vol. 7, 113 810–113 825, 2019.

[30] CVX Research, Inc., CVX: MATLAB software for disciplined convex programming, version 2.0, http://cvxr.com/cvx, Apr. 2011.

[31] Chen, K., X. Yun, Z. He, and C. Han, "Synthesis of sparse planar arrays using modified real genetic algorithm," *IEEE Transactions on Antennas and Propagation*, Vol. 55, No. 4, 1067–1073, 2007.